remote sensing

MDPI

Technical Note

Satellite-Derived Estimate of City-Level Methane Emissions from Calgary, Alberta, Canada

Zhenyu Xing [1,*], Thomas E. Barchyn [1], Coleman Vollrath [1], Mozhou Gao [1,2] and Chris Hugenholtz [1]

[1] Centre for Smart Emissions Sensing Technologies, University of Calgary, Calgary, AB T2N 1N4, Canada; tbarchyn@ucalgary.ca (T.E.B.); coleman.vollrath1@ucalgary.ca (C.V.); mozhou.gao@sensorup.com (M.G.); chhugenh@ucalgary.ca (C.H.)
[2] Sensorup Inc., Calgary, AB T2G 1S5, Canada
* Correspondence: zhenyu.xing2@ucalgary.ca

Abstract: Cities are important sources of anthropogenic methane emissions. Municipal governments can play a role in reducing those emissions to support climate change mitigation, but they need information on the emission rate to contextualize mitigation actions and track progress. Herein, we examine the application of satellite data from the TROPOspheric Monitoring Instrument (TROPOMI) to estimate city-level methane emission rates in a case study of the City of Calgary, Alberta, Canada. Due to low and variable annual observational coverage, we integrated valid TROPOMI observations over three years (2020–2022) and used mass balance modeling to derive a long-term mean estimate of the emission rate. The resulting column-mean dry-air mole fraction (XCH_4) enhancement over Calgary was small (4.7 ppb), but within the city boundaries, we identified local hot spots in the vicinity of known emission sources (wastewater treatment facilities and landfills). The city-level emission estimate from mass balance was 215.4 ± 132.8 t CH_4/d. This estimate is approximately four times larger than estimates from Canada's gridded National Inventory Report of anthropogenic CH_4 emissions and six times larger than the Emissions Database for Global Atmospheric Research (EDGAR v8.0). We note that valid TROPOMI observations are more common in warmer months and occur during a narrow daily overpass time slot over Calgary. The limited valid observations in combination with the constrained temporal observational coverage may bias the emission estimate. Overall, the findings from this case study highlight an approach to derive a screening-level estimate of city-level methane emission rates using TROPOMI data in settings with low observational coverage.

Keywords: methane; TROPOMI; mass balance; emission estimate; city level

Citation: Xing, Z.; Barchyn, T.E.; Vollrath, C.; Gao, M.; Hugenholtz, C. Satellite-Derived Estimate of City-Level Methane Emissions from Calgary, Alberta, Canada. *Remote Sens.* **2024**, *16*, 1149. https://doi.org/10.3390/rs16071149

Academic Editors: Janne Hakkarainen and Alexander Kokhanovsky

Received: 14 February 2024
Accepted: 18 March 2024
Published: 26 March 2024

1. Introduction

Reduction in methane (CH_4) emissions is considered an effective near-term pathway to reduce anthropogenic greenhouse gas emissions that exacerbate climate change [1,2]. CH_4 emissions from the energy (e.g., oil and gas production and coal mining), agriculture (rice cultivation and feedlots), and waste (landfills) sectors are three major sources of anthropogenic CH_4 [3–7].

Urban areas, in particular, are very poorly understood sources of CH_4 emissions due to the large diversity of sources. In urban areas, wastewater treatment facilities and landfills are generally well known to be large emitters [8–11]. However, urban areas also contain many smaller, widely distributed sources such as leaks in natural gas (NG) distribution infrastructure, small-scale agriculture, sewer emissions, natural gas vehicles, and slip from NG combustion [8,12–16]. Most of these sources are poorly understood and may vary considerably in emission characteristics and rates.

Due to the diversity and number of sources across urban areas, conventional bottom-up (BU) CH_4 emission inventories are normally inaccurate. There are considerable challenges associated with maintaining and implementing BU inventories in urban areas as inventories must model both the number of discrete emission sources and predict appropriate

emission rates. Granular BU inventory models in urban environments will always carry considerable uncertainty. And by extension, inventory-based mitigation policy will be inherently inefficient as this uncertainty carries through to policy decisions.

To reduce the uncertainty of BU inventories and understand if BU inventories are adequately simulating emissions, it is helpful to use larger-scale top-down (TD) measurements. Measurements of atmospheric concentrations of CH_4 in urban areas can be carried out with platforms such as ground-based stations and networks, vehicle- and aircraft-based systems, and satellites, e.g., [17–23]. The measurement resolution varies substantially from the equipment level to the basin level depending on the platform. The TD approach uses these measurements with atmospheric transport modeling to estimate emission rates and help understand the fidelity of BU estimates.

Among TD methods, satellites are of particular interest. The high observational density and large-scale geographic coverage of the TROPOspheric Monitoring Instrument (TROPOMI) on board the Copernicus Sentinel-5 Precursor satellite provides one of the best options for satellite TD measurements. Multiple approaches have been proposed and used to estimate urban CH_4 emissions using TROPOMI observations, including transport inversion, two-dimensional Gaussian modeling, and tracer–tracer approaches [10,23–25]. Based on CH_4 measurements from a multi-tiered observing framework (including observations from TROPOMI, an aircraft-based system, and ground-based stations), Cusworth et al. [24] used geostatistical inverse modeling and prior emissions to estimate CH_4 emissions from the Los Angeles megacity. De Foy et al. [10] used a two-dimensional Gaussian model with TROPOMI observations and estimated CH_4 emissions from 61 urban areas globally. The tracer–tracer method, which quantifies emissions by scaling the ratios of prior estimates of CH_4:CO or CH_4:CO_2 with atmospheric measurements, has been used to estimate CH_4 emission rates from urban centers in North America [23,25].

The majority of the city-level CH_4 emission estimate methods require high observational coverage and fine spatial resolution [26,27]. For urban areas in Canada, it is more challenging to use TROPOMI observations to estimate the city-level CH_4 emissions because of the relatively low number of valid observations and the small sizes of the urban areas. In this case study of the City of Calgary, we explore the feasibility of TROPOMI to estimate the city-level CH_4 emission rate and present an approach using data integration to overcome low observational coverage. We integrated all valid observations during the 3-year period from 2020 and 2022 and applied the mass balance method of Buchwitz et al. [28] to derive a long-term screening-level estimate of Calgary's CH_4 emission rate. We explore the context of these measurements relative to existing inventories and estimates from other cities. We also examine how the characteristics of the TROPOMI satellite in high-latitude settings could influence representative emission estimates.

2. Materials and Methods

2.1. Study Area

Calgary is located in southern Alberta in the transitional area between the foothills of the Rocky Mountains and the North American Great Plains. In 2021, Calgary covered a land area of 820.62 km^2 [29]. The city center coordinates are 51.04° (latitude) and −114.06° (longitude). Calgary's population in 2022 was 1.4 million [30]. The urban area bordered by the City of Calgary's municipal boundaries is shown in Figure 1. In our work, the entire urban area was predefined as the source region and further screened using the TROPOMI-observed CH_4 enhancements.

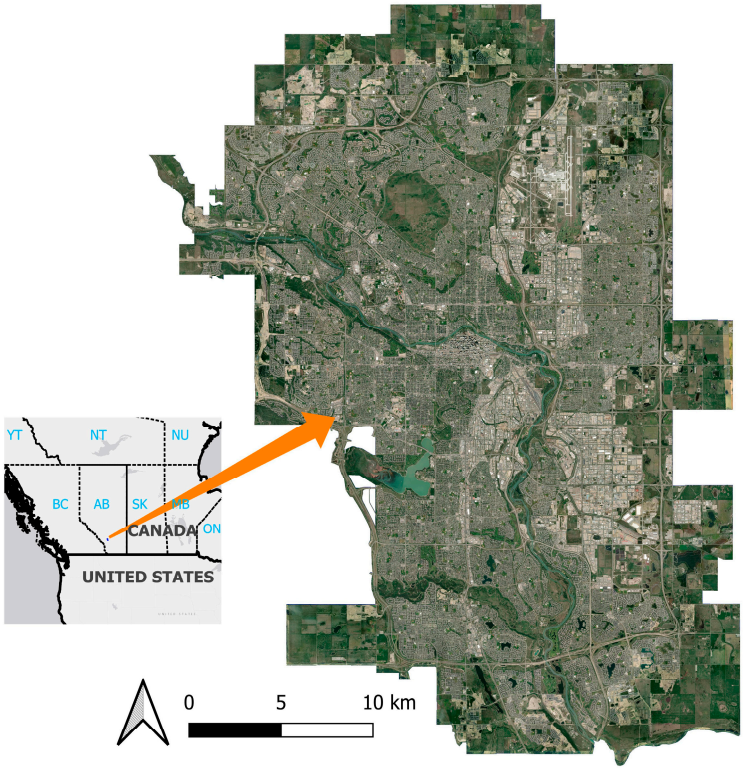

Figure 1. Spatial extent of the City of Calgary and its location in the context of Western Canada.

2.2. TROPOMI CH_4 Observation

As the only payload on Sentinel-5P (S5P), TROPOMI is a nadir-viewing push-broom grating hyperspectral spectrometer with a field-of-view of 108°. TROPOMI covers wavelengths of ultraviolet–visible (UV-VIS, 270 nm to 495 nm), near-infrared (NIR, 675 nm to 775 nm), and shortwave infrared (SWIR, 2305 nm–2385 nm) [31]. The operational S5P Level-2 processor employs the RemoTeC full-physics algorithm to retrieve the atmospheric CH_4 content from Earth radiance measurements in the NIR and SWIR spectral bands [32,33]. Independent validation by the S5P Mission Performance Centre and the S5P Validation Team concluded that the CH_4 total column data have good overall agreement with reference measurements collected from a global network of ground-based stations (e.g., Total Carbon Column Observing Network and Network for the Detection of Atmospheric Composition Change) and the data products from other satellite platforms (i.e., Japanese Greenhouse Gases Observing Satellite) [32,33]. The retrieved atmospheric CH_4 content is provided as the column-mean dry air mixing ratio of CH_4 (XCH_4, ppb) in the TROPOMI Level-2 data product. To correct the underestimation of the TROPOMI XCH_4 data for low albedo, bias-corrected XCH_4 is also provided in the data product.

The data used in this work included 3 years of the TROPOMI Level-2 data product, which spanned the period from 1 January 2020 to 31 December 2022. The spatial resolution of all observations in this work is 7 km × 5.5 km. For each observation, the bias-corrected XCH_4 value and corresponding retrieval quality indicator "qa_value" were extracted from the data for analysis. In this study, only high-quality, bias-corrected XCH_4 values were used (hereafter: valid observations), as indicated by qa_value > 0.5. The overpass time of TROPOMI for Calgary was between 12:00 p.m. and 14:00 p.m. local time. The 3-year mean XCH_4 observations from 2020–2022 at 0.05° × 0.05° resolution were obtained from all valid observations during the study period.

The data processing procedure is summarized in Figure 2. Since the original TROPOMI XCH_4 data products are provided with a non-normalized grid, the first step was to develop a normalized 0.05° × 0.05° latitude-longitude grid (hereafter: pixel) for reallocation of multiple observations. For each individual observation, every valid XCH_4 data point

(i.e., qa_value > 0.5) was reallocated onto the pixel that corresponded with its geolocation. This process was conducted using a TROPOMI daily screening toolkit developed by Gao et al. [34].

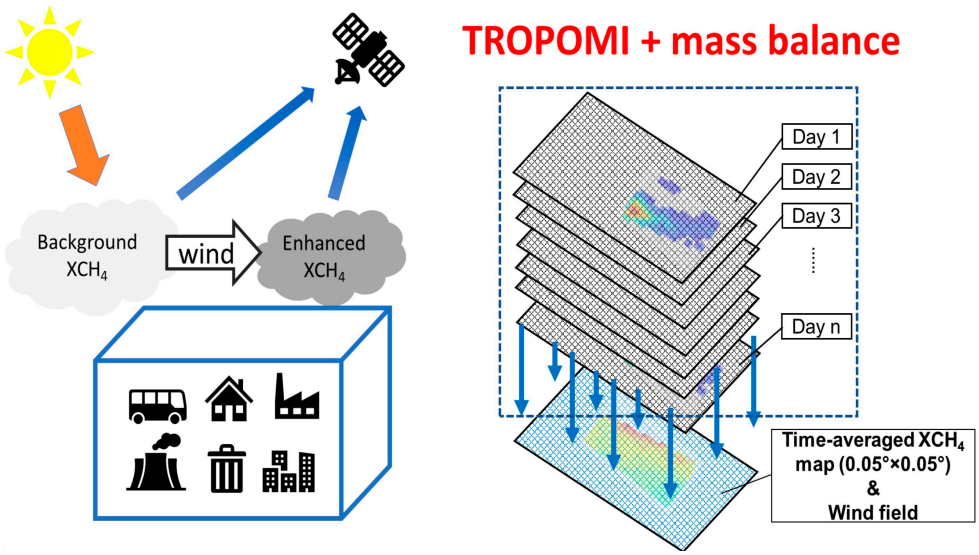

Figure 2. Diagram of air mass transport through source regions (**left**) and composite of multiple valid TROPOMI observations (**right**).

The second step involved screening the number of valid observations per pixel in 2020, 2021, and 2022 for both the source region (City of Calgary boundary) and the surrounding region used to determine the background XCH_4 (Figure 3). This step was used to assess the coverage of the valid TROPOMI observations for subsequent processing to derive the emission rate estimate. Coverage describes the sample size of valid observations per pixel and within the source and surrounding regions and the temporal distribution of valid observations throughout the year. Generally, confidence in the CH_4 emission hotspot screening and emission rate estimate increases with increasing coverage. Considering the diversity of CH_4 sources in urban areas (e.g., landfills, natural gas point-sources, and end-use incomplete combustion), coverage should ideally capture variations in the characteristics and rates of emissions from these sources across space and through time. Therefore, as coverage increases, the representativeness of CH_4 emission rate estimates for the study period should improve.

Figure 3 indicates variable year-to-year and month-to-month coverage within the source and surrounding regions for the study period. The lowest coverage was in 2020, and all the pixels of the source region contained <10 valid observations. Coverage improved in 2021 but varied spatially, particularly with less valid observations over the source region. Coverage was higher and least variable in 2022. Monthly variations were also noted (Figure 3e). Five months in 2020 had no valid observations, and in all three years, there were no valid observations in December and January. In general, summer and fall had the highest coverage.

Given the year-to-year and month-to-month variations, we integrated the data from 2020–2022 to increase the sample size for emission quantification. By doing so, all pixels within the source and surrounding region were covered by at least 17 valid observations. We averaged the XCH_4 in each pixel across the valid observations. The 3-year mean XCH_4 map was then denoised using Gaussian filters prior to emission quantification. Filtering was completed using a 2D Gaussian smoothing kernel with a standard deviation of 1 and a filter size of 3.

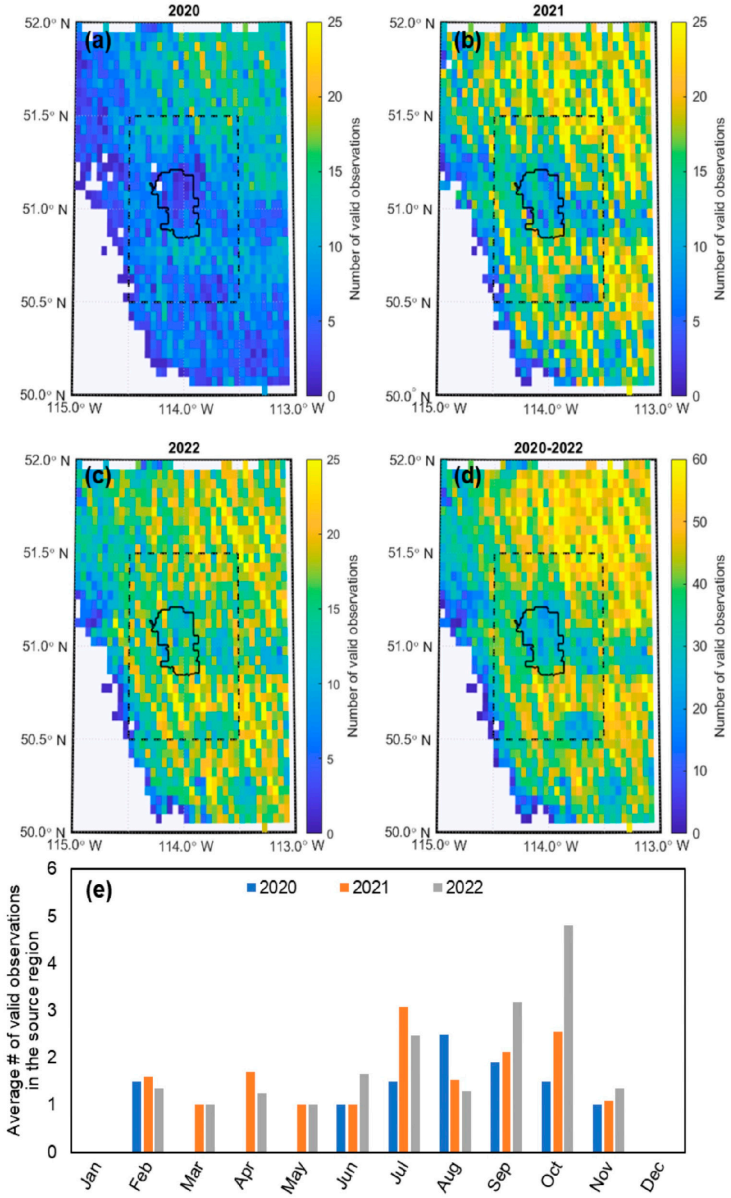

Figure 3. Spatial–temporal variations in the TROPOMI valid coverage: (**a**–**c**) the annual coverage in 2020, 2021, and 2022, respectively; (**d**) the integrated 3-year coverage in 2020–2022; (**e**) the monthly average number of valid observations in the source region. For panel (**a**–**d**), the solid black line denotes the source region (City of Calgary) boundary, while the dotted black line denotes the surrounding region for the background XCH_4 estimate.

2.3. Emission Quantification: Mass Balance Model

We used the method proposed by Buchwitz et al. [28] to estimate the city-level CH_4 emission rate. The method uses mass balance theory to build an integrated emission rate estimate from multiple TROPOMI data scenes. From the underlying theory, an air parcel with background XCH_4 travels through the source region (characterized by the effective length, L, calculated as the square root of source region area) as directed by the wind speed, V. It is assumed that the XCH_4 of the air parcel is enhanced as determined by the accumulation time, τ (duration of the air parcel travelling through the source region, calculated as L/V), and the emission rate (Q, mass per time) in the source region. The CH_4 column mass enhancement (ΔmCH_4, CH_4 mass per area) is calculated as $(Q \times \tau)/L^2$. It is assumed that when travelling through the source region, ΔmCH_4 increases linearly. Therefore, the mean column mass enhancement over the source region can be calculated

as $0.5 \times \Delta mCH_4$, where ΔmCH_4 is calculated from the observed XCH_4 by introducing a factor, M, with the unit of $kgCH_4/(km^2 \times ppb)$. As a result, the modeled column mass enhancement and the observation-based column mass enhancement are connected. The basic equation is as follows:

$$Q = \Delta XCH_4 \times CF \quad (1)$$

where the ΔXCH_4 is the CH_4 enhancement in ppb, derived from the 3-year mean XCH_4 map and CF denotes the conversion factor to convert the CH_4 enhancement over the source region to the emission rate, Q. CF is calculated from the following Equation (2):

$$CF = M \times M_{exp} \times L \times V \times C \quad (2)$$

where M is the factor to convert the atmospheric total column mixing ratio to mass change per area for standard conditions (i.e., surface pressure at 1013.0 hPa), which is 5.345 kg $CH_4/(km^2 \times ppb)$; L (km) is the effective length of the source region; V (km/d) is the ventilation wind speed during the TROPOMI overpass derived from in situ measurements at multiple air monitoring stations in the Calgary urban area; C is a unitless factor of 2.0, which is the assumed linear increase in CH_4 column mass enhancement of the air parcel when travelling over the source region [28]; and M_{exp} is a dimensionless factor to correct for the actual mass, calculated using the following equation:

$$M_{exp} = \frac{\langle M_i \rangle}{M} \approx \frac{\langle p_i \rangle}{1013.0} \quad (3)$$

where p_i is the surface pressure of the i-th pixel (in hPa), which is obtained from the 3dimensional monthly mean in the MERRA-2 reanalysis data product [35]; $\langle\ \rangle$ denotes averaging over all pixels of the source region; and 1013.0 refers to the surface pressure (hPa) under standard conditions.

Background XCH_4 is required to calculate ΔXCH_4 over the source region. Background XCH_4 can be estimated using XCH_4 upwind of the study region or a statistical approach [29]. The number of valid upwind observations may be insufficient to provide a robust estimate of background XCH_4 given impeding factors such as cloud cover, surface albedo, and aerosol optical depth [26]. Similarly, given that background XCH_4 is non-homogenous in large study regions, background estimates derived with the statistical approach can be biased. Lauvaux et al. [36] proposed an optimized statistical background XCH_4 estimation approach in their study of global CH_4 ultra-emitters using noisy satellite imagery. Briefly, for a region with ultra-emitting CH_4 plumes, the computation of the background XCH_4 value is sensitive to the skewness of the XCH_4 values, determined by $\left(\overline{x}_{XCH_4} - \mu_{XCH_4}\right)/\sigma_{XCH_4}/$, where $\overline{x}_{XCH_4}$, μ_{XCH_4}, and σ_{XCH_4} are the mean, median, and standard deviation of the XCH_4 values in the region. Thus, as indicated by Equation (4), for regions with highly skewed XCH_4, the background is computed as μ_{XCH_4}. Otherwise, the background is computed as $l \times \mu_{XCH_4} - (l-1) \times \overline{x}_{XCH_4}$, where l is an empirical parameter that has been used to segment emission hotspots. To maximize the probability of emission hotspot segmentation, the value of l is typically 2.5 [36].

In this work, we adopted the statistical approach of Lauvaux et al. [36] to estimate the background XCH_4. Here, the source region (i.e., City of Calgary) replaces the ultra-emitters present in Lauvaux et al.'s study [36]. A broader region surrounding the source region was then used to calculate the background XCH_4. The size of the surrounding region was defined based on a compromise between several conditions to: (i) limit contributions from other anthropogenic sources of CH_4 emissions outside the source region, (ii) ensure similar or better coverage than in the source region, and (iii) avoid areas with no valid observations. According to these conditions, the surrounding region was defined as a rectangular area centered on the source region with latitude range from 50.5° to 51.5° and longitude range from −114.5° to −113.5°, as indicated by the dashed outlines on the maps in Figure 3.

The pixel-specific CH_4 enhancement, ΔXCH_4, was derived by subtracting background XCH_4 from the 3-year mean XCH_4 for each pixel in the source region. Pixels with $\Delta XCH_4 < \sigma_{XCH_4}$ were not considered as source pixels and were therefore not included in the calculation of ΔXCH_4. This was performed to exclude pixels with ΔXCH_4 biased by the regional variation in XCH_4.

$$XCH_{4,background} = \begin{cases} \mu_{XCH_4},\ if\ \frac{\overline{x}_{XCH_4} - \mu_{XCH_4}}{\sigma_{XCH_4}} > 0.3 \\ 2.5\ \times \mu_{XCH_4} - 1.5 \times \overline{x}_{XCH_4},\ if\ \frac{\overline{x}_{XCH_4} - \mu_{XCH_4}}{\sigma_{XCH_4}} \leq 0.3 \end{cases} \quad (4)$$

Uncertainty in the emission estimate (σ) in this work mainly comes from the uncertainty in the calculations of ΔXCH_4, $\sigma_{\Delta XCH_4}$, and the conversion factor CF (σ_{CF}). Therefore, we applied the law of propagation of uncertainty [36,37] and calculated σ as the combined uncertainty of $\sigma_{\Delta XCH_4}$ and σ_{CF} in the source region (e.g., Equation (5)). The main contributor to σ_{CF} is uncertainty in wind speed. In this work, σ_{CF} was assumed equivalent to σ_V, and was estimated from the temporal variation in wind speed during averaging. The calculations of $\sigma_{\Delta XCH_4}$ and σ_{CF} are indicated by Equations (6) and (7), respectively.

$$\sigma = \sqrt{\sigma^2_{\Delta XCH_4} + \sigma^2_{CF}} \quad (5)$$

$$\sigma_{\Delta XCH_4} = \sigma_{XCH_4} \times M \times M_{exp} \times L \times V \times C \quad (6)$$

$$\sigma_{CF} = \Delta XCH_4 \times M \times M_{exp} \times L \times \sigma_V \times C \quad (7)$$

3. Results and Discussion

3.1. Methane Enhancements

Figure 4 shows maps of the mean XCH_4 and ΔXCH_4 over the source region. Figure 4a shows that the mean XCH_4 per pixel within the source region was higher than the surrounding region. Within the source region, higher XCH_4 areas were found in central and northeast Calgary (Figure 4b). The mean XCH_4 in the source region was 1879.1 $\pm$ 2.7 ppb, while the mean and median XCH_4 within the surrounding region were 1873.3 ppb and 1874.5 ppb. The background XCH_4 estimated using Equation (4) was 1876.3 ppb. It should be noted that not all pixels within the source region were found to have elevated XCH_4. Therefore, the calculated mean XCH_4 for the City of Calgary does not exhibit substantially higher XCH_4 compared to the background XCH_4.

Pixel-specific enhancements, ΔXCH_4, were derived by subtracting the background XCH_4 from the observed XCH_4 (Figure 4b). Only the pixels with enhancements greater than the standard deviation (2.7 ppb) were defined as 'sources' within the source region. The mean ΔXCH_4 from the 'sources' was 4.7 ppb. The highest enhancement (7.4 ppb) was over central Calgary near one of three active landfills. There are 23 facilities in Calgary that are required to report annual CH_4 emissions to Canada's Greenhouse Gas Reporting Program (GHGRP). As indicated in Figure 4b, nearly all of the facilities (21/23) were located within the XCH_4 enhanced areas as determined in our analysis.

Compared to TROPOMI-based ΔXCH_4 estimates from other urban areas in North America [10], the mean ΔXCH_4 in Calgary from 2020–2022 is near the upper end of city-level enhancements derived from cities with similar populations (Figure 5). For the 18 cities with populations of less than 5 million, ΔXCH_4 does not noticeably correlate with the population. Although Calgary's population is only half of Toronto (Canada), our TROPOMI-based ΔXCH_4 estimate for Calgary (4.7 ppb) is slightly higher than that estimated by de Foy et al. [10] for Toronto (4.5 ppb). It should be noted that for de Foy et al. [10], ΔXCH_4 for the urban areas studied was estimated based on a two-dimensional Gaussian fit method and not strictly constrained by the city boundaries. Thus, different ΔXCH_4 estimation methods may introduce bias.

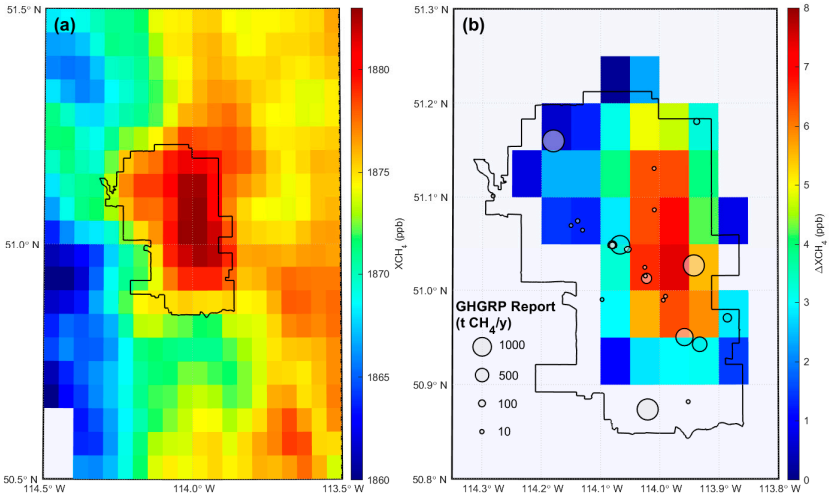

Figure 4. Maps of XCH_4 and ΔXCH_4 over the City of Calgary source region between 1 January 2020 and 31 December 2022: (**a**) 2020–2022 average XCH_4 for the source and surrounding regions and (**b**) 2020–2022 average ΔXCH_4 for the source region (only showing pixels with positive enhancements). The source region (City of Calgary) boundary is indicated by the solid black line. Facilities reporting to Canada's Greenhouse Gas Reporting Program (GHGRP) are indicated by the blue circles in panel (**b**), with the size denoting the emission magnitude (t CH_4/y).

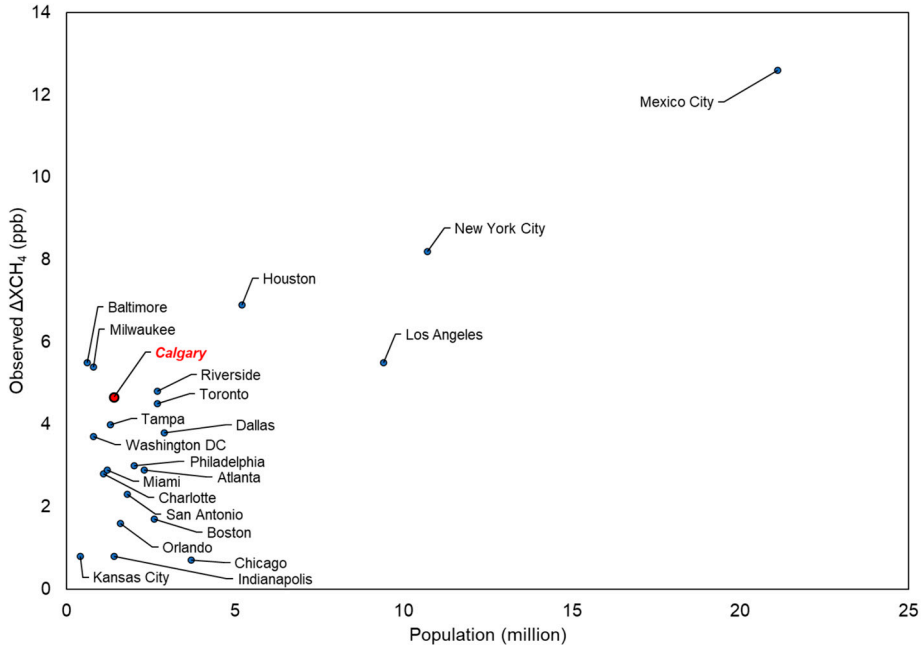

Figure 5. TROPOMI-based city-level ΔXCH_4 from select cities in North America. Data for all cities but data for Calgary were derived from the work conducted by de Foy et al. [10], which relied on a two-dimensional Gaussian model for ΔXCH_4 calculations.

3.2. City-Level CH_4 Emission Rate and Comparisons with BU Inventories

Using the mass balance method, we calculated Calgary's 3-year mean emission rate as 215.4 t CH_4/d with an uncertainty of 132.8 t CH_4/d over the period 2020–2022. The uncertainty is dominated by $\sigma_{\Delta XCH_4}$ (111.2 t CH_4/d). The large $\sigma_{\Delta XCH_4}$ is mainly attributed to spatial variations in ΔXCH_4 (Figure 4b). As discussed in Buchwitz et al. [28], spatial variations in emissions over the source region can bias the emission estimate. The uncertainty associated with wind observations was smaller (72.6 t CH_4/d) and may reflect the potential bias caused by the temporal variations in wind speed in the source region during the study period. Therefore, the uncertainty of 132.8 t CH_4/d in this work indicates the

extent to which our emission estimate may be biased by the spatial and temporal variations in the emissions sources and wind speed in Calgary, respectively.

Figure 6 shows TROPOMI-based city-level CH_4 emission estimates for select North American cities [10,23]. In general, the emission rate increases with population. Compared to CH_4 emission rate estimates from other major cities, Calgary's emission rate is relatively low but comparable with cities that have slightly lower and higher emissions and populations, respectively (e.g., Portland, Charlotte, Kansas City, Washington, DC, and Baltimore). Although the city-level emission estimates were all derived from TROPOMI observations, the methods used to quantify emissions varied and differed from the mass balance method in this work. Plant et al. [23] used the tracer–tracer ratio approach (ΔCH_4:ΔCO), while de Foy et al. [10] used a two-dimensional Gaussian fit method. The noticeable discrepancies between the emission estimates by Plant et al. [23] and de Foy et al. [10] for the same cities (e.g., New York City, Mexico City, Boston, and Baltimore) imply that measurement-based, city-level CH_4 emission estimates are methodologically dependent. For current and emerging satellite-based platforms capable of measuring CH_4, it is crucial to establish a suite of proven and well-tested emission quantification approaches to improve confidence and enable direct comparisons between estimates.

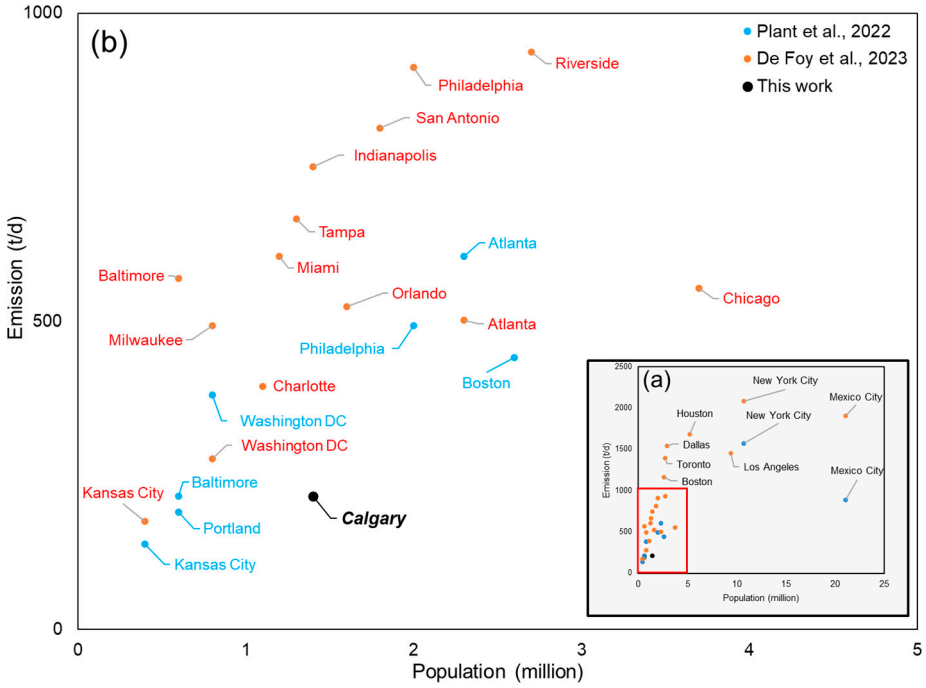

Figure 6. City-level CH_4 emissions for select North American cities using TROPOMI-based estimates from de Foy et al. [10] and Plant et al. [23]: (**a**) overall distribution of the city-level CH4 emissions for the investigated cities and (**b**) zoom-in view of the bottom left cluster in panel (**a**). The emission rate estimates are based on the three different quantification methods reported by each study. Population data for Calgary were obtained from the Government of Alberta open data [30].

City-level CH_4 emission estimates from BU emission inventories are much lower than our measurement-based estimate. Table 1 lists the city-level CH_4 emission rates in Calgary from several gridded emission inventories and emissions reported to Canada's Greenhouse Gas Reporting Program (GHGRP). The most recent EDGAR inventory (i.e., v8.0) estimates annual city-level CH_4 emissions for Calgary at 31.6 t CH_4/d (2020), 38.2 t CH_4/d (2021), and 34.9 t CH_4/d (2022), with a mean of 34.9 t CH_4/d. Canada's gridded national inventory report (NIR) of anthropogenic CH_4 emissions estimated 48.3 t CH_4/d for Calgary in 2018 [38]. This is higher than the EDGARv8.0 estimates but still only accounts for less than one quarter of the measurement-based estimate reported herein using TROPOMI. The mismatch between the BU emissions inventories and the TROPOMI-based estimate from this study is

consistent with the discrepancies observed between inventory and measurement-based estimates of CH_4 emissions for other major cities in North America [10,23,25,39].

Table 1. City-level CH_4 emission rate estimates for Calgary.

Data Source	Emission Rate (t CH_4/d)	Year
EDGARv8.0	31.6	2020
EDGARv8.0	38.2	2021
EDGARv8.0	34.9	2022
EDGARv8.0	34.9	2020–2022
Gridded NIR	48.3	2018
GHGRP [1]	20.3	2020–2021
This work	215.4 ± 132.8	2020–2022

[1] Only includes sources with annual emission rates > 10 kt CO_2-eq.

Canada's GHGRP collects information on greenhouse gas emissions annually from facilities across Canada. As a mandatory program, facilities that emit 10 kilotonnes (kt) or more in carbon dioxide equivalent (CO_2-eq) units per year, must report their emissions to Environment and Climate Change Canada [40]. A total of 23 facilities reporting to the GHGRP within Calgary's city limits averaged 20.3 CH_4/d between 2020 and 2021, which is 9.4% of the emission estimate using TROPOMI data and 42.1% and 58.2% of total inventoried emissions in the gridded NIR and EDGARv8.0, respectively. The large gap between the GHGRP-reported emissions, BU emission inventories, and our measurement-based estimate suggests that Calgary's emissions profile is dominated by CH_4 sources below the GHGRP reporting threshold of 10 kt CO_2e-eq/year or emissions from those sources are under-reported. Overall, our results highlight the need for a re-examination of the emissions factors, activity factors, and methods used to develop BU inventories and expansion of the facilities covered by GHGRP requirements.

3.3. Observational Bias

As suggested by EDGARv8.0, there is modest seasonal variation in Calgary's CH_4 emissions, with slightly lower emissions in the summer than in the winter (Figure 7a). This is consistent with measurement-based estimates from the Baltimore and Washington, DC, metropolitan region in the U.S. [41]. Urban CH_4 sources (e.g., slip from incomplete combustion of natural gas at end-use, landfills, and wastewater treatment) are characterized by noteworthy temporal variations related to natural gas consumption, barometric pressure, temperature, and moisture [42–45]. It is possible that different emissions processes compete and dominate the city-level emissions profile at different times of the year. The valid TROPOMI observations for Calgary were mainly constrained to the period from June to October in each year. The higher observational coverage during summer and fall may fail to capture the CH_4 emission characteristics of other sources in other months of the year and thus bias the TROPOMI-based emission estimate.

As a supplemental indicator, the monthly natural gas consumption of City of Calgary-owned facilities was included in Figure 7a to examine potential seasonality- and temperature-induced fluctuation in CH_4 emissions related to natural gas end-use. Generally, EDGARv8.0 CH_4 emissions are higher in colder months and appear to correlate to some degree with the natural gas consumption data. For context, the main fuel used for space heating in the City of Calgary is natural gas. We used the EDGARv8.0 emission variability to seasonally correct our Calgary estimate from 215.4 ± 132.8 t CH_4/d to 220.1 t CH_4/d. Compared to the large uncertainty surrounding our mean estimate, this correction has little impact on the magnitude of the city-level emission rate estimate. The limitation of using the seasonality from EDGARv8.0 to temporally correct our estimate is that inventories have known issues with underestimating CH_4 emissions compared to measurement-based estimates. Therefore, it is challenging to draw more definitive conclusions on annual emissions using TROPOMI data because the observations are temporally constrained.

Another noteworthy point of using TROPOMI observations is the fixed sensing time slot on each day for Calgary. TROPOMI's overpass time slot for Calgary is between 12:00–14:00 local time. For sources with strong diurnal variations, the fixed observation time may result in marked uncertainty when scaling up emission rate estimates from hourly to daily/monthly/annual. Measurement-based emission rate estimates conducted in London, UK, show the highest emission flux around 12:00 p.m. with a maximum-to-minimum ratio of 1.9 [46]. Figure 7b shows the average hourly variations in CH_4 concentrations from three ground-based air monitoring stations in Calgary. The data show that CH_4 concentrations are lower during the TROPOMI overpass time slot. Furthermore, the TROPOMI overpass time for Calgary spans typical work hours during the week. CH_4 emission measurements from a sensor mounted on a light-rail transit platform in Salt Lake Valley, Utah, found temporal variations in emissions from a manufacturing facility [47]. Plumes from this facility were only detectable during work hours. Similar sources of emissions likely exist in Calgary. This introduces more uncertainty into scaling the hourly emission rate up to an annual rate, as emission patterns from different sources may fluctuate between days/evenings, weekdays/weekends, and holidays.

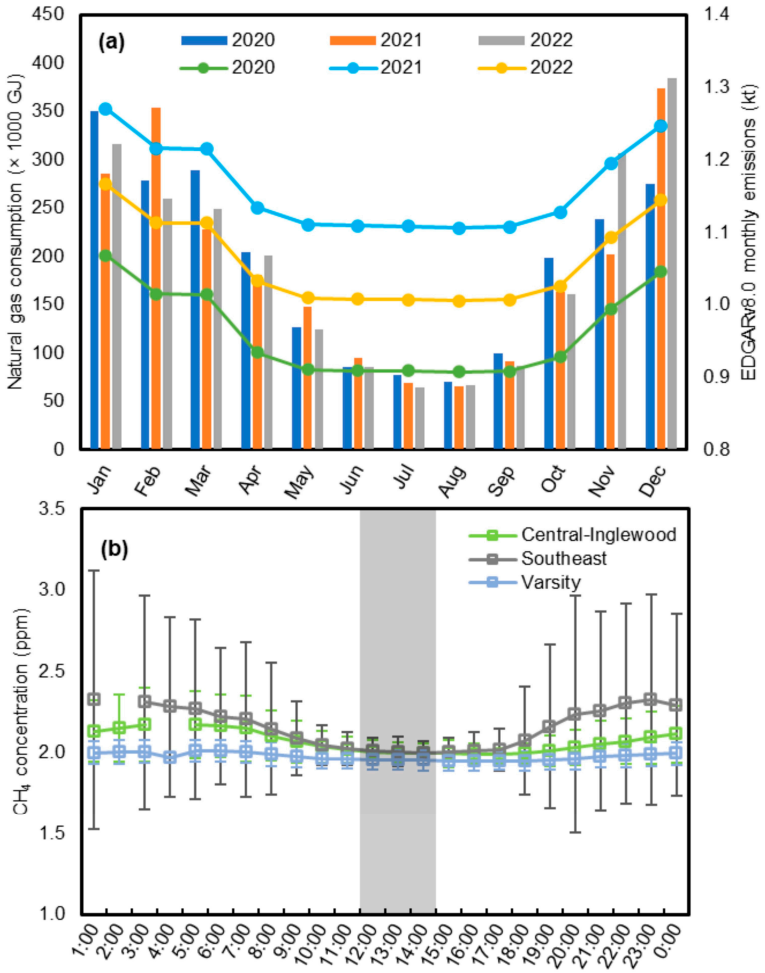

Figure 7. Temporal variations in CH_4 emissions and sources in the City of Calgary: (**a**) monthly natural gas consumption data for City of Calgary facilities (bar) and BU inventory estimates from EDGAR v8.0 (line) and (**b**) average hourly (local time) CH_4 concentration levels from three air monitoring stations for the period from June to October in 2020, 2021, and 2022. Natural gas consumption data were obtained from the City of Calgary open data [48]. Continuous hourly ground-level CH_4 concentration measurements were retrieved from the Alberta Air Data Warehouse [49]. The shaded time slot in (**b**) is the TROPOMI overpass time for Calgary.

The long-term mean CH_4 emission rate estimated from the mass balance method is relatively robust to poor satellite coverage but is well acknowledged to be less accurate than more complex methods because of the simplified transport algorithm. It is important to emphasize that our estimate for Calgary carries considerable uncertainty (see Buchwitz et al. [28] for an extensive discussion of the uncertainties inherent to the mass balance method). The observational bias discussed in this work likely introduces additional uncertainties in the CH_4 emission estimate. It is possible to correct this observational bias with support from BU emissions inventories, but inventories suffer from known issues, and thus, such corrections may be unreliable. Despite the observational bias inherent in our estimate, our results suggest that inventories may not be accurately estimating Calgary's total CH_4 emissions and that emissions may be considerably higher.

4. Conclusions

In this work, we explored the feasibility of using TROPOMI observations and the mass balance method of Buchwitz et al. [28] to estimate a city-level CH_4 emission rate for Calgary, Alberta, Canada—a city with low annual satellite observational coverage. To overcome the low observational coverage from TROPOMI in Calgary, we integrated all valid observations from 2020–2022. The 3-year mean TROPOMI XCH_4 observations revealed elevated XCH_4 within the study area. Pixels of elevated XCH_4 overlapped with the distribution of larger, well-known CH_4 sources in Calgary. The mean XCH_4 enhancement from the pixels within the study area was 4.7 ppb.

The mean emission rate estimate for Calgary between 2020–2022 was 215.4 ± 132.8 t CH_4/d. This estimate falls on the lower end of other TROPOMI-based CH_4 emission rate estimates of other major North American cities and is comparable with the magnitude of emissions in cities with similar populations. Consistent with the findings of previous studies, the gaps between our TROPOMI-based city-level CH_4 emission rate estimate and BU inventories suggest that the latter are underestimating CH_4 emissions from the City of Calgary. Evidence shows that city-level CH_4 emissions in general (and Calgary specifically) are higher than initially predicted, but the exact source of the discrepancy cannot be reliably determined from these data. Future research to better understand the emissions profile of Calgary (and by extension, similar urban areas) with more granular measurements is warranted. BU inventories may not be accounting for all sources of CH_4 emissions, activity factors could be inaccurate, or some combination of the two. Thus, research to catalogue all potential sources of CH_4 emissions in cities may lead to better modeling and more accurate inventory estimates.

Our analysis shows that TROPOMI observations of CH_4 emissions from Calgary are biased to warmer months and are performed over a fixed daily time slot. As such, this bias likely introduces uncertainty into our emission estimate. Future work will assess whether more complex models or other data and methods can be used to correct this bias for cities like Calgary with limited satellite coverage.

Author Contributions: Conceptualization, Z.X., C.V., T.E.B. and C.H.; methodology, Z.X. and M.G.; data curation and formal analysis, Z.X.; writing—original draft preparation, Z.X., T.E.B. and C.H.; writing—review and editing, Z.X., C.V., T.E.B., M.G. and C.H.; visualization, Z.X. and M.G.; supervision, C.H.; project administration, C.H.; funding acquisition, C.H. All authors have read and agreed to the published version of the manuscript.

Funding: This project was undertaken with the financial support of the Government of Canada. Ce project a été réalisé avec l'appui financier du gouvernement du Canada.

Data Availability Statement: The datasets used in this work are publicly accessible as follows: The TROPOMI L2 methane observations data products are available at: https://disc.gsfc.nasa.gov/datasets/S5P_L2__CH4____HiR_2/summary?keywords=Sentinel-5P%20TROPOMI (accessed on 18 October 2023); the Modern-Era Retrospective analysis for Research and Applications version 2 (MERRA-2) datasets are available at: https://disc.gsfc.nasa.gov/datasets/M2IMNPASM_5.12.4/summary?keywords=wind (accessed on 19 October 2023); the EDGARv8.0 GHG emissions

datasets are available at: https://edgar.jrc.ec.europa.eu/dataset_ghg80 (accessed on 4 January 2024); the ground-based stationary continuous monitoring data of methane in Calgary are available at: https://data-donnees.az.ec.gc.ca/data/air/monitor/national-air-pollution-surveillance-naps-program/Data-Donnees/?lang=en (accessed on 20 November 2023); and the natural gas consumption data of City of Calgary facilities are available at: https://data.calgary.ca/Environment/Primary-Natural-Gas-Usage/s5g9-8sgf (accessed on 4 December 2023). The TROPOMI data processing toolkit is available at: https://github.com/MozhouGao/TROPOMI_Daily_Screening_Toolkit.git (accessed on 20 November 2023).

Acknowledgments: The authors thank the EDGAR team for the publicly accessible Global Greenhouse Gas emissions database (EDGARv8.0 products); the TROPOMI team for the publicly accessible TROPOMI L2 data products; and NASA Goddard Earth Sciences (GES) Data and Information Services Center (DISC) for providing the easily accessible data platform.

Conflicts of Interest: Author Mozhou Gao is currently employed by Sensorup Inc. The remaining authors declare that the research was conducted in the absence of any commercial or financial relationships that could be construed as a potential conflict of interest.

References

1. Shoemaker, J.K.; Schrag, D.P.; Molina, M.J.; Ramanathan, V. What role for short-lived climate pollutants in mitigation policy? *Science* **2013**, *342*, 1323–1324. [CrossRef] [PubMed]
2. Nisbet, E.G.; Manning, M.R.; Dlugokencky, E.J.; Fisher, R.E.; Lowry, D.; Michel, S.E.; Myhre, C.L.; Platt, S.M.; Allen, G.; Bousquet, P.; et al. Very strong atmospheric CH_4 growth in the 4 years 2014–2017: Implications for the Paris Agreement. *Glob. Biogeochem. Cycles* **2019**, *33*, 318–342. [CrossRef]
3. Yusuf, R.O.; Noor, Z.Z.; Abba, A.H.; Hassan, M.A.A.; Din, M.F.M. CH_4 emission by sectors: A comprehensive review of emission sources and mitigation methods. *Renew. Sustain. Energy Rev.* **2012**, *16*, 5059–5070. [CrossRef]
4. Zhang, Y.; Gautam, R.; Pandey, S.; Omara, M.; Maasakkers, J.D.; Sadavarte, P.; Lyon, D.; Nesser, H.; Sulprizio, M.P.; Varon, D.J.; et al. Quantifying CH_4 emissions from the largest oil-producing basin in the United States from space. *Sci. Adv.* **2020**, *6*, 5120. [CrossRef] [PubMed]
5. Kholod, N.; Evans, M.; Pilcher, R.C.; Roshchanka, V.; Ruiz, F.; Coté, M.; Collings, R. Global CH_4 emissions from coal mining to continue growing even with declining coal production. *J. Clean. Prod.* **2020**, *256*, 120489. [CrossRef] [PubMed]
6. Jiang, Y.; Qian, H.; Huang, S.; Zhang, X.; Wang, L.; Zhang, L.; Shen, M.; Xiao, X.; Chen, F.; Zhang, H.; et al. Acclimation of CH_4 emissions from rice paddy fields to straw addition. *Sci. Adv.* **2019**, *5*, 9038. [CrossRef] [PubMed]
7. Maasakkers, J.D.; Varon, D.J.; Elfarsdóttir, A.; McKeever, J.; Jervis, D.; Mahapatra, G.; Pandey, S.; Lorente, A.; Borsdorff, T.; Foorthuis, L.R.; et al. Using satellites to uncover large CH_4 emissions from landfills. *Sci. Adv.* **2022**, *8*, 9683. [CrossRef] [PubMed]
8. Cambaliza, M.O.; Shepson, P.B.; Bogner, J.E.A.N.; Caulton, D.R.; Stirm, B.; Sweeney, C.; Montzka, S.A.; Gurney, K.R.; Spokas, K.; Salmon, O.E.; et al. Quantification and source apportionment of the methane emission flux from the city of Indianapolis. *Elementa* **2015**, *3*, 000037. [CrossRef]
9. Ars, S.; Vogel, F.; Arrowsmith, C.; Heerah, S.; Knuckey, E.; Lavoie, J.; Lee, C.; Pak, N.M.; Phillips, J.L.; Wunch, D. Investigation of the spatial distribution of methane sources in the greater Toronto area using mobile gas monitoring systems. *Environ. Sci. Technol.* **2020**, *54*, 15671–15679. [CrossRef]
10. de Foy, B.; Schauer, J.J.; Lorente, A.; Borsdorff, T. Investigating high methane emissions from urban areas detected by TROPOMI and their association with untreated wastewater. *Environ. Res. Lett.* **2023**, *18*, 044004. [CrossRef]
11. Nesser, H.; Jacob, D.J.; Maasakkers, J.D.; Lorente, A.; Chen, Z.; Lu, X.; Shen, L.; Qu, Z.; Sulprizio, M.P.; Winter, M.; et al. High-resolution US methane emissions inferred from an inversion of 2019 TROPOMI satellite data: Contributions from individual states, urban areas, and landfills. *EGUsphere* **2023**, 1–36. [CrossRef]
12. Cui, Y.Y.; Brioude, J.; McKeen, S.A.; Angevine, W.M.; Kim, S.W.; Frost, G.J.; Ahmadov, R.; Peischl, J.; Bousserez, N.; Liu, Z.; et al. Top-down estimate of methane emissions in California using a mesoscale inverse modeling technique: The South Coast Air Basin. *J. Geophys. Res. Atmos.* **2015**, *120*, 6698–6711. [CrossRef]
13. Chamberlain, S.D.; Ingraffea, A.R.; Sparks, J.P. Sourcing methane and carbon dioxide emissions from a small city: Influence of natural gas leakage and combustion. *Environ. Pollut.* **2016**, *218*, 102–110. [CrossRef]
14. Hopkins, F.M.; Kort, E.A.; Bush, S.E.; Ehleringer, J.R.; Lai, C.T.; Blake, D.R.; Randerson, J.T. Spatial patterns and source attribution of urban CH_4 in the Los Angeles Basin. *J. Geophys. Res. Atmos.* **2016**, *121*, 2490–2507. [CrossRef]
15. Fischer, M.L.; Chan, W.R.; Delp, W.; Jeong, S.; Rapp, V.; Zhu, Z. An estimate of natural gas methane emissions from California homes. *Environ. Sci. Technol.* **2018**, *52*, 10205–10213. [CrossRef]
16. Hajny, K.D.; Salmon, O.E.; Rudek, J.; Lyon, D.R.; Stuff, A.A.; Stirm, B.H.; Kaeser, R.; Floerchinger, C.R.; Conley, S.; Smith, M.L.; et al. Observations of methane emissions from natural gas-fired power plants. *Environ. Sci. Technol.* **2019**, *53*, 8976–8984. [CrossRef]
17. Hopkins, F.M.; Ehleringer, J.R.; Bush, S.E.; Duren, R.M.; Miller, C.E.; Lai, C.T.; Hsu, Y.K.; Carranza, V.; Randerson, J.T. Mitigation of CH_4 emissions in cities: How new measurements and partnerships can contribute to emissions reduction strategies. *Earth's Future* **2016**, *4*, 408–425. [CrossRef]

18. Ren, X.; Salmon, O.E.; Hansford, J.R.; Ahn, D.; Hall, D.; Benish, S.E.; Stratton, P.R.; He, H.; Sahu, S.; Grimes, C.; et al. CH_4 emissions from the Baltimore-Washington area based on airborne observations: Comparison to emissions inventories. *J. Geophys. Res. Atmos.* **2018**, *123*, 8869–8882. [CrossRef]
19. Goldsmith Jr, C.D.; Chanton, J.; Abichou, T.; Swan, N.; Green, R.; Hater, G. Methane emissions from 20 landfills across the United States using vertical radial plume mapping. *J. Air Waste Manag.* **2012**, *62*, 183–197. [CrossRef]
20. Okorn, K.; Jimenez, A.; Collier-Oxandale, A.; Johnston, J.; Hannigan, M. Characterizing methane and total non-methane hydrocarbon levels in Los Angeles communities with oil and gas facilities using air quality monitors. *Sci. Total Environ.* **2021**, *777*, 146194. [CrossRef]
21. Ryoo, J.M.; Iraci, L.T.; Tanaka, T.; Marrero, J.E.; Yates, E.L.; Fung, I.; Michalak, A.M.; Tadić, J.; Gore, W.; Bui, T.P.; et al. Quantification of CO_2 and CH_4 emissions over Sacramento, California, based on divergence theorem using aircraft measurements. *Atmos. Meas. Tech.* **2019**, *12*, 2949–2966. [CrossRef]
22. Miller, S.M.; Wofsy, S.C.; Michalak, A.M.; Kort, E.A.; Andrews, A.E.; Biraud, S.C.; Dlugokencky, E.J.; Eluszkiewicz, J.; Fischer, M.L.; Janssens-Maenhout, G.; et al. Anthropogenic emissions of CH_4 in the United States. *P. Natil. Acad. Sci.* **2013**, *110*, 20018–20022. [CrossRef] [PubMed]
23. Plant, G.; Kort, E.A.; Murray, L.T.; Maasakkers, J.D.; Aben, I. Evaluating urban CH_4 emissions from space using TROPOMI CH_4 and carbon monoxide observations. *Remote Sens. Environ.* **2022**, *268*, 112756. [CrossRef]
24. Cusworth, D.H.; Duren, R.M.; Yadav, V.; Thorpe, A.K.; Verhulst, K.; Sander, S.; Hopkins, F.; Rafiq, T.; Miller, C.E. Synthesis of methane observations across scales: Strategies for deploying a multitiered observing network. *Geophys. Res. Lett.* **2020**, *47*, 2020GL087869. [CrossRef]
25. Plant, G.; Kort, E.A.; Floerchinger, C.; Gvakharia, A.; Vimont, I.; Sweeney, C. Large fugitive CH_4 emissions from urban centers along the US East Coast. *Geophys. Res. Lett.* **2019**, *46*, 8500–8507. [CrossRef] [PubMed]
26. Gao, M.; Xing, Z.; Vollrath, C.; Hugenholtz, C.H.; Barchyn, T.E. Global observational coverage of onshore oil and gas CH_4 sources with TROPOMI. *Sci. Rep.* **2023**, *13*, 16759. [CrossRef] [PubMed]
27. Jacob, D.J.; Varon, D.J.; Cusworth, D.H.; Dennison, P.E.; Frankenberg, C.; Gautam, R.; Guanter, L.; Kelley, J.; McKeever, J.; Ott, L.E.; et al. Quantifying methane emissions from the global scale down to point sources using satellite observations of atmospheric methane. *Atmos. Chem. Phys.* **2022**, *22*, 9617–9646. [CrossRef]
28. Buchwitz, M.; Schneising, O.; Reuter, M.; Heymann, J.; Krautwurst, S.; Bovensmann, H.; Burrows, J.P.; Boesch, H.; Parker, R.J.; Somkuti, P.; et al. Satellite-derived CH_4 hotspot emission estimates using a fast data-driven method. *Atmos. Chem. Phys.* **2017**, *17*, 5751–5774. [CrossRef]
29. Statistics Canada. Census Profile. 2021 Census of Population. Statistics Canada Catalogue no. 98-316-X2021001. Ottawa. Released. Available online: https://www12.statcan.gc.ca/census-recensement/2021/dp-pd/prof/index.cfm?Lang=E (accessed on 29 January 2024).
30. Government of Alberta Open Data: Population by Municipality. 2023. Available online: https://open.alberta.ca/opendata/population-by-municipality (accessed on 12 December 2023).
31. Landgraf, J.; Lorente, A.; Langerock, B.; Sha, M.K. S5P Mission Performance Centre Methane [L2_CH4_] Readme. 2020. Available online: https://sentinel.esa.int/documents/247904/3541451/Sentinel-5P-Methane-Product-Readme-File (accessed on 27 April 2022).
32. Hu, H.; Hasekamp, O.; Butz, A.; Galli, A.; Landgraf, J.; Aan de Brugh, J.; Borsdorff, T.; Scheepmaker, R.; Aben, I. The operational methane retrieval algorithm for TROPOMI. *Atmos. Meas. Tech.* **2016**, *9*, 5423–5440. [CrossRef]
33. Lorente, A.; Borsdorff, T.; Butz, A.; Hasekamp, O.; Schneider, A.; Wu, L.; Hase, F.; Kivi, R.; Wunch, D.; Pollard, D.F.; et al. Methane retrieved from TROPOMI: Improvement of the data product and validation of the first 2 years of measurements. *Atmos. Meas. Tech.* **2021**, *14*, 665–684. [CrossRef]
34. Gao, M.; Xing, Z. TROPOMI Daily Screening Toolkit—Version 1.0. Available online: https://github.com/MozhouGao/TROPOMI_Daily_Screening_Toolkit.git (accessed on 20 November 2023).
35. Global Modeling and Assimilation Office (GMAO). *MERRA-2 instM_3d_asm_Np: 3d, Monthly Mean, Instantaneous, Pressure-Level, Assimilation, Assimilated Meteorological Fields V5.12.4*; Goddard Earth Sciences Data and Information Services Center (GES DISC): Greenbelt, MD, USA, 2015. [CrossRef]
36. Lauvaux, T.; Giron, C.; Mazzolini, M.; d'Aspremont, A.; Duren, R.; Cusworth, D.; Shindell, D.; Ciais, P. Global assessment of oil and gas CH_4 ultra-emitters. *Science* **2022**, *375*, 557–561. [CrossRef]
37. Pandey, S.; Houweling, S.; Lorente, A.; Borsdorff, T.; Tsivlidou, M.; Bloom, A.A.; Poulter, B.; Zhang, Z.; Aben, I. Using satellite data to identify the methane emission controls of South Sudan's wetlands. *Biogeosciences* **2021**, *18*, 557–572. [CrossRef]
38. Scarpelli, T.R.; Jacob, D.J.; Moran, M.; Reuland, F.; Gordon, D. A gridded inventory of Canada's anthropogenic CH_4 emissions. *Environ. Res. Lett.* **2021**, *17*, 014007. [CrossRef]
39. Pitt, J.R.; Lopez-Coto, I.; Hajny, K.D.; Tomlin, J.; Kaeser, R.; Jayarathne, T.; Stirm, B.H.; Floerchinger, C.R.; Loughner, C.P.; Gately, C.K.; et al. New York City greenhouse gas emissions estimated with inverse modeling of aircraft measurements. *Elem. Sci. Anth.* **2022**, *10*, 00082. [CrossRef]
40. Environment and Climate Change Canada (ECCC) Greenhouse Gas Reporting Program (GHGRP)—Facility Greenhouse Gas (GHG) Data. Available online: https://open.canada.ca/data/en/dataset/a8ba14b7-7f23-462a-bdbb-83b0ef629823 (accessed on 24 November 2023).

41. Huang, Y.; Kort, E.A.; Gourdji, S.; Karion, A.; Mueller, K.; Ware, J. Seasonally resolved excess urban methane emissions from the Baltimore/Washington, DC metropolitan region. *Environ. Sci. Technol.* **2019**, *53*, 11285–11293. [CrossRef] [PubMed]
42. Bogner, J.E.; Spokas, K.A.; Chanton, J.P. Seasonal greenhouse gas emissions (methane, carbon dioxide, nitrous oxide) from engineered landfills: Daily, intermediate, and final California cover soils. *J. Environ. Qual.* **2011**, *40*, 1010–1020. [CrossRef]
43. Xu, L.; Lin, X.; Amen, J.; Welding, K.; McDermitt, D. Impact of changes in barometric pressure on landfill methane emission. *Glob. Biogeochem. Cycles* **2014**, *28*, 679–695. [CrossRef]
44. Masuda, S.; Suzuki, S.; Sano, I.; Li, Y.Y.; Nishimura, O. The seasonal variation of emission of greenhouse gases from a full-scale sewage treatment plant. *Chemosphere* **2015**, *140*, 167–173. [CrossRef]
45. Cambaliza, M.O.L.; Bogner, J.E.; Green, R.B.; Shepson, P.B.; Harvey, T.A.; Spokas, K.A.; Stirm, B.H.; Corcoran, M. Field measurements and modeling to resolve m^2 to km^2 CH_4 emissions for a complex urban source: An Indiana landfill study. *Elem. Sci. Anth.* **2017**, *5*, 36. [CrossRef]
46. Helfter, C.; Tremper, A.H.; Halios, C.H.; Kotthaus, S.; Bjorkegren, A.; Grimmond, C.S.B.; Barlow, J.F.; Nemitz, E. Spatial and temporal variability of urban fluxes of methane, carbon monoxide and carbon dioxide above London, UK. *Atmos. Chem. Phys.* **2016**, *16*, 10543–10557. [CrossRef]
47. Mitchell, L.E.; Crosman, E.T.; Jacques, A.A.; Fasoli, B.; Leclair-Marzolf, L.; Horel, J.; Bowling, D.R.; Ehleringer, J.R.; Lin, J.C. Monitoring of greenhouse gases and pollutants across an urban area using a light-rail public transit platform. *Atmos. Environ.* **2018**, *187*, 9–23. [CrossRef]
48. City of Calgary, Primary Natural Gas Usage. Available online: https://data.calgary.ca/Environment/Primary-Natural-Gas-Usage/s5g9-8sgf (accessed on 17 November 2023).
49. Government of Alberta: Alberta Air Data Warehouse. Available online: https://www.alberta.ca/alberta-air-data-warehouse (accessed on 17 November 2023).